

See discussions, stats, and author profiles for this publication at: <https://www.researchgate.net/publication/259348475>

Non-Exponential Kinetics and a Complete Folding Pathway of an α -Helical Heteropeptide: Direct Observation and Comprehensive Molecular Dynamics

ARTICLE *in* THE JOURNAL OF PHYSICAL CHEMISTRY B · DECEMBER 2013

Impact Factor: 3.3 · DOI: 10.1021/jp410934g · Source: PubMed

CITATIONS

2

READS

35

3 AUTHORS:



Gouri S. Jas

Central University of the Caribbean

44 PUBLICATIONS 1,826 CITATIONS

[SEE PROFILE](#)



Charles Russell Middaugh

University of Kansas

371 PUBLICATIONS 9,283 CITATIONS

[SEE PROFILE](#)



Krzysztof Kuczera

University of Kansas

116 PUBLICATIONS 14,351 CITATIONS

[SEE PROFILE](#)

Non-Exponential Kinetics and a Complete Folding Pathway of an α -Helical Heteropeptide: Direct Observation and Comprehensive Molecular Dynamics

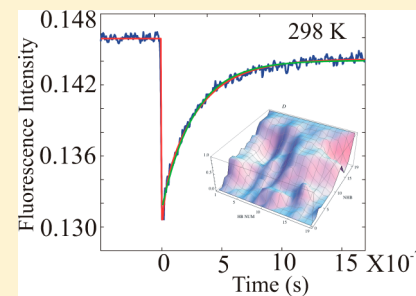
Gouri S. Jas,^{*,†} C. Russell Middaugh,[†] and Krzysztof Kuczera^{*,‡}

[†]Department of Pharmaceutical Chemistry, The University of Kansas, Lawrence, Kansas 66047, United States

[‡]Department of Chemistry and Department of Molecular Biosciences, The University of Kansas, Lawrence, Kansas 66045, United States

Supporting Information

ABSTRACT: We have performed a combined experimental and computational study of the folding of a 21-residue α -helix-forming heteropeptide (WH21). Temperature jump kinetics with improved dynamic range at several temperatures revealed non-exponential relaxation that could be well described with two time constants of 20 and 300 ns at 298 K. In the computational part, we performed multi-microsecond molecular dynamics simulations of WH21 in explicit water, using the AMBER03 and OPLS/AA potentials. The simulations were in good agreement with available experimental data on helix content and relaxation times. On the basis of 70 individual transitions, we identified the main pathways of helix unfolding. Three paths were found in both force fields, with unfolding progressing through (1) N-terminus, C-terminus, and center; (2) C-terminus, N-terminus, and center; and (3) C-terminus, center, and N-terminus. An additional fourth path starting in the central region and expanding to the termini was detected only with AMBER03. Intermediate structures sampled along the pathway included a central helix with frayed termini, an off-center helix, and a helical hairpin. The simulations suggest that the short relaxation should be assigned to partly cooperative fluctuations of several neighboring hydrogen bonds. Overall, by a combination of ultrafast kinetic measurements and detailed microscopic description through comprehensive molecular dynamics, we have obtained important new insights into the helix folding process.



INTRODUCTION

Secondary structure formation is the foundation that governs the folding of proteins.¹ Developments of spectroscopic techniques have made it possible to investigate the kinetics of α -helix formation in peptides from 21 to 5 residues in length.² Although intensive studies from both experimental and theoretical perspectives have been devoted to the dynamics of this secondary structural element, the microscopic details of the helix–coil transition are yet to clearly emerge. Atomistic computer simulations with very long trajectories have the potential to provide a wide range of information about this process, yielding the sought after conformational transition pathways and rates, including capturing of rarely sampled intermediates.³ The progress in computational studies of peptide dynamics and folding has been achieved with improvements in methodology and in increased complexity of treated systems. Early studies with direct molecular dynamics (MD) and free energy simulations of secondary structure elements^{3c} were followed by extensive simulations of helices, sheets, and miniproteins with first implicit and later explicit solvent models.^{3b,c} Significant progress was obtained by employing replica-exchange simulations that generated predictions of helix melting curves, showing that hydrogen bonds were more stable in the peptide center than at the termini, and that shielding by side chain atoms stabilized neighboring backbone hydrogen

bonds.^{3b,4} Our recent simulations using REMD confirmed that current force fields yield correct helix content and suggested the presence of an “off-center” intermediate for the 21-residue WH21 peptide.^{3a} In terms of kinetics, a number of helix folding studies employed implicit solvent.⁵ A major effort using distributed computing was undertaken by Pande et al. who found helix folding initiation at multiple nucleation sites, followed by extension of several helix fragments and their merging into a single helix.⁶ Direct molecular dynamics simulations in explicit solvent have been successfully employed to model folding kinetics of short helical peptides,^{2g,7} also including effects of salt.⁸ Additionally, the specialized algorithm of milestone was used to describe folding of longer helices along predefined paths⁹ and for shorter helices in terms of a kinetic network.^{2g}

Experimentally, alanine rich peptides of moderate size have been found to form stable isolated helices in solution at a physiologically relevant pH.^{2c,10} More recently, helix formation was detected in blocked pentapeptides, Ac-WA₃H⁺-NH₂ (WH₅) and Ac-A₅-NH₂ (acA₅a) at moderate pH,^{7b} in contrast to previous data for unblocked alanine systems under very low pH

Received: November 6, 2013

Revised: December 14, 2013

Published: December 16, 2013

conditions.¹¹ Experimental progress has also been achieved in probing residue-specific dynamics and thermodynamics of isotopically labeled peptides with IR spectroscopy. Thus, a higher melting temperature was detected in the central part of the helix compared to the termini,¹² variations of about 10% in relaxation time were detected for four-residue sections at different locations,¹³ and relaxations of individual hydrogen bonds were found to span an order of magnitude in a constrained helix.^{5c} The availability of short helix-forming model peptides is of crucial importance, allowing application of both computational and experimental approaches to these interesting systems. However, the microscopic details of the mechanism of helix formation are still largely unknown.

In the present study, we apply the nanosecond laser temperature jump technique^{2c,14} to the WH21 peptide, Ac-WAAAH(AAARA)₃-A-NH₂. Formation of the first helical turn in WH21 is signaled by quenching of tryptophan (W) fluorescence by the protonated histidine (H). Temperature jump kinetics detected the presence of a faster component of 20 ns, along with a slower component of 300 ns at 298 K. The existence of a faster component for this peptide was previously observed using an ultrafast laser temperature jump measurement but was not captured in its entirety due to the short 5 ns dynamic range.^{2f} The longer component from the kinetic measurements corresponds to the overall helix-coil relaxation dynamics, while the faster component may be attributed to helix nucleation or more generally to formation of *folding intermediate(s)*. In the computational part of this study, we perform long-term MD simulations of WH21 in explicit solvent, generating a 16.9 μ s trajectory with the AMBER03 force field and 13.0 μ s with OPLS/AA. Our simulations yield helix populations and kinetic constants comparable to the experimental data, and additionally provide information about the detailed pathways of helix formation and suggest that the short experimental time events may be assigned to correlated relaxation of groups of neighboring hydrogen bonds.

METHODS

Experimental: Materials. The peptide, 21-residue helical heteropeptide WH21, was purchased from GenScript USA Inc., NJ. As determined from HPLC, the purity was greater than 98%. The N and C termini of the peptide are acetylated and amidated, respectively. There are 22 peptide bonds in this peptide including the N and C terminal caps.

Experimental: Temperature Jump Kinetics. The instrument used in the temperature jump experiments has been described in detail elsewhere.^{2b,c,15} The initial rapid decrease results from a change in the intrinsic tryptophan fluorescence due to the change in temperature. Temperature jumps of 8–10 K were generated by absorption of a near-infrared laser pulse (1.54 μ m) by the aqueous solution. The time dependence of the fluorescence intensity was monitored to measure the kinetics. Trp was excited using a continuous ultraviolet probe beam (264 nm), and the emitted light was monitored using band-pass filters which transmitted wavelengths from 320 to 400 nm. The kinetic experiments were carried out in a 0.05 \times 1.0 cm² cuvette at a sample concentration of \sim 100 μ M in 20 mM acetate buffer at pH 4.8. Measured kinetics for the change in fluorescence of the WH21 heteropeptide were recorded over the temperature range 278–308 K.

Computational: Systems and Simulations. The simulated system was the peptide Ac-WAAAH⁺(AAARA)₃-A-NH₂. The N-terminal was acetylated, the C-terminal was amidated,

and the histidine residue was in the protonated form, corresponding to acidic pH conditions. The initial coordinates were constructed in an ideal helix conformation using CHARMM.¹⁶ Two main simulations were performed, using the AMBER03¹⁷ and OPLS/AA¹⁸ force fields. In the AMBER03 simulation, the peptide was solvated with 3587 TIP3P water molecules and 8 Na⁺ and 12 Cl⁻ ions were added to create a neutral system close to physiological ionic strength in a cubic box of initial size 48 Å. After a brief energy minimization, 10 ps MD with constrained peptide and 100 ps of free MD at 320 K and 1 bar, a trajectory of 16.9 μ s was generated at a constant temperature of 320 K, controlled by the velocity-scaling algorithm¹⁹ and under constant volume conditions, with the box size fixed at 48.7 Å. A cutoff of 10 Å was used for the van der Waals interactions and for direct electrostatic interactions, and the PME method was employed to treat long-range electrostatic interactions. In the OPLS/AA simulation, the peptide was solvated by 3563 TIP3P waters, with 4 Cl⁻ ions added for system neutrality. After brief energy minimization, 10 ps MD with constrained peptide and 100 ps MD at 300 K and 1 bar, a 13.0 μ s trajectory was generated at a constant temperature, controlled by velocity-scaling and constant volume with fixed box side of 48.2 Å. The cutoff for the van der Waals interactions was 14 Å, the cutoff for direct electrostatic interactions was 10 Å, and the PME method was employed to treat long-range electrostatic interactions.²⁰ The simulations were performed with the GROMACS program,¹⁹ using a 2 fs time step with constraints on all bond lengths. Using 36 CPUs in parallel, about 100 ns per day were generated on the Kodiak cluster at Baylor University.

Computational: Trajectory Analysis. Helix population was analyzed in two ways: the HB method, counting the number of $i\cdots i+4$ backbone hydrogen bonds with O \cdots N distances below 3.6 Å, and the PP method, counting the number of residues within a 20° radius of the ideal structure (φ, ψ) = (-62°, -41°). Due to the presence of blocking groups, the WH21 peptide can form 19 α -helical hydrogen bonds, with HB1 involving the carbonyl O of the acetyl blocking group and N of Ala4 and HB19 the carbonyl O of Ala18 and the N of the amide blocking group. Kinetic parameters were calculated primarily from autocorrelation functions (ACFs) of fluctuations—for $C\alpha$ root-mean-square deviation (RMSD) from the ideal helix, end-to-end distance (EEDIS), distance between centers of mass of the Trp and His side chains (WHDIS), and the average fluctuations of individual hydrogen bond lengths (HB). Fitting the ACFs to multiexponential decays directly yielded estimates of the relaxation times τ_r . The individual pathways for helix-coil transitions were quite complex and diverse, with individual hydrogen bonds executing multiple local fluctuations during each global transition. To simplify pathway analysis, we employed a “last time of visit” approach. Thus, from a trajectory fragment corresponding to a helix (NHB = 19) to coil (NHB = 0) transition, we saved snapshots of the last visit to NHB = 19, 18, 17, ..., 1 and first visit to NHB = 0. The reverse procedure was followed for coil to helix transitions. This gave a schematic picture of each transition by providing a single structure for each value of the total number of helical hydrogen bonds NHB. Records of individual transitions are presented in the Supporting Information. Statistical errors of calculated quantities were typically obtained by dividing trajectories into several consecutive fragments and finding the standard deviation of the mean at the 95% confidence level.

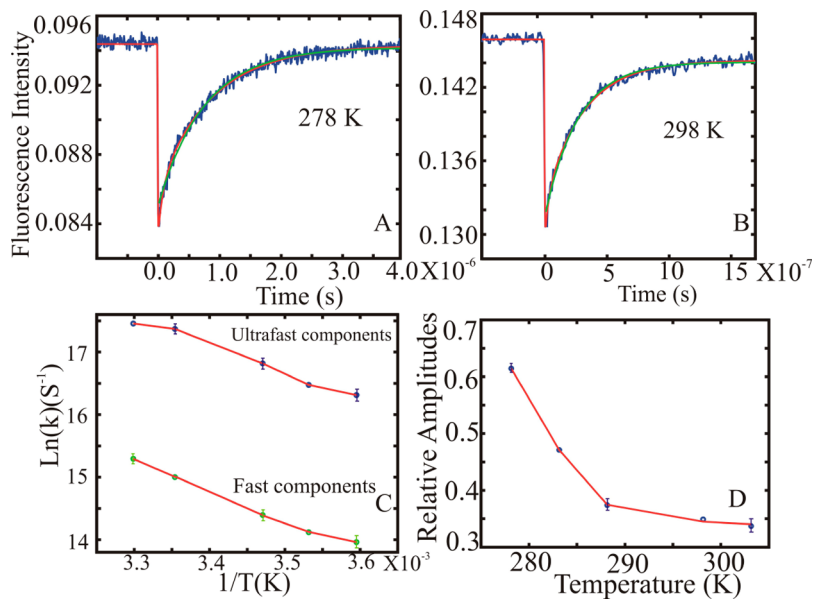


Figure 1. Kinetics from the change in fluorescence of WH21. Data are shown for the final temperature 278 K (A) and 298 K (B). Fluorescence intensity is plotted in arbitrary units. Fit to the data with single-exponential (green) and double-exponential function (red) for 298 K. The sample concentration is $\sim 100 \mu\text{M}$. A summary plot for the temperature-dependent relaxation rates in Arrhenius form (log of rate vs $1/T$; in solid blue; ultrafast component, and in solid green; fast component, circles with error bar) in part C and the relative amplitude of the fast phase (solid blue with error bar) in part D. Error estimates are larger for the ultrafast components at higher temperatures due to their decreasing amplitudes.

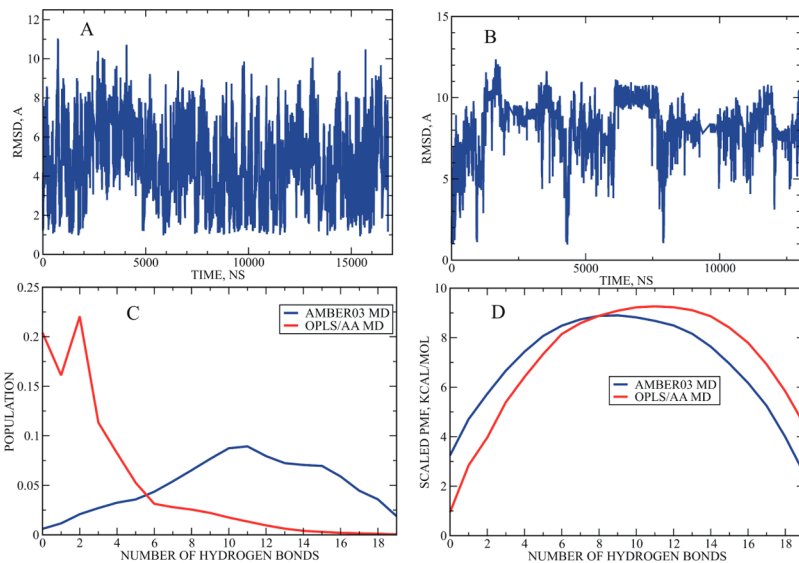


Figure 2. C α RMSD from an ideal helix: (A) 16.9 μs AMBER03 MD at 320 K; (B) 13 μs OPLS/AA MD at 300 K. (C) Distribution of the number of formed hydrogen bonds in MD trajectories. (D) Same distribution converted to PMF and scaled by the number of states $C(r) = 19!/r!(19 - r)!$.

RESULTS AND DISCUSSION

Experimental Section. Experimental results are shown in Figure 1. For the temperature-jump kinetics, fits to two-exponential decays were significantly improved over single-exponentials, with χ^2 values typically 2 orders of magnitude lower (Figure 1A,B). The relaxation times τ_1 (fast) and τ_2 (slow) are 20 and 300 ns at 25 °C (298 K) and 10 and 210 ns at 35 °C (308 K), respectively (Figure 1C). The ratio of amplitudes of the faster to the slower decays is given in Figure 1D, showing a decreasing contribution of the fast component with increasing temperature. Using two-state kinetics and the previously determined helix content of 44% at 300 K,^{2c} the 300 ns relaxation corresponds to a 680 ns folding time and a 540 ns unfolding time.

Computational. Helix Content. The population of the helical conformation found in the MD trajectories was $16 \pm 5\%$ (PP method) and $16 \pm 6\%$ (HB method) in the OPLS/AA trajectory at 300 K and $55 \pm 4\%$ (PP method) and $57\% \pm 6\%$ (HB method) in the AMBER03 trajectory at 320 K. These results are comparable to the experimental results of 44% helix at 300 K and 18% helix at 320 K.^{2c} The MD results are very similar to our previous REMD simulations, with the AMBER03 force field tending to overestimate and OPLS/AA underestimating the helix content.^{3a} A similar helix content of 62% at 300 K was recently found for a 12-residue peptide, Ace-AEAAAKEAAAKA-Nme with AMBER03.⁸ While most molecular mechanics force fields are able to correctly reproduce helix content at room

temperature, they have difficulty with reproducing helix melting curves.²¹

Sampled Conformers. The time evolution of the RMSD of trajectory structures from the ideal helix is shown in Figure 2A,B, demonstrating the occurrence of multiple helix–coil transitions. In a coarse-grained picture, we can consider our WH21 peptide with 19 helical hydrogen bonds as having $2^{19} = 524\,288$ backbone conformations. Of these, one corresponds to the ideal helix ($\text{NHB} = 19$) and one to the ideal coil ($\text{NHB} = 0$), with a majority exhibiting intermediate folding; e.g., for $\text{NHB} = 9$ and 10, the number of conformers is $19!/10!9! = 92\,378$. Sampled conformer distributions as a function of NHB are shown in Figure 2C,D. In the AMBER03 trajectory, we sampled 122 746 (23%) of these 2^{19} states. The majority of the sampled conformers corresponded to folding intermediates with $\text{NHB} = 8–16$, with low populations of both end points—0.6% for $\text{NHB} = 0$ and 2.2% for $\text{NHB} = 19$. In the OPLS/AA MD, we sampled 54 215 (10%) out of the coarse-grained conformers, with a majority of sampled structures corresponding to unfolded states with $\text{NHB} = 0–4$, and populations of 19.6% for $\text{NHB} = 0$ and only 0.07% for $\text{NHB} = 19$. In conclusion, we sampled a wide range of conformers, with a majority exhibiting intermediate stages of folding. When compared to the random sampling model, in which the probability of forming r hydrogen bonds is $19!/r!(19 - r)!$, the intermediate states are actually under-sampled, and we can think of folding as a two-state process with a transition between the stable helix and coil states and a single barrier with a maximum at ca. 12 (AMBER03) or 8 (OPLS/AA) hydrogen bonds (Figure 2D).

Kinetics. Kinetic parameters extracted from autocorrelation functions of several variables are shown in Table 1 and in Figure

Table 1. Kinetic Time Constants from MD Simulations of WH21^a

	AMBER03, 320 K		OPLS/AA, 300 K	
	τ_1	τ_2	τ_1	τ_2
RMSD C ₁	3	60	16	270
EEDIS C ₁	1	50	16	220
HB C ₁	9	88	12	240
WHDIS C ₁	2	50	11	120

^aUnits: ns. Estimates of statistical errors: about 40% for AMBER03 results and 50% for the OPLS/AA values. C₁: RMSD, EEDIS, HB, WHDIS time constants obtained from two-exponential fits to decays of autocorrelation functions describing fluctuations around average for Ca RMSD from helix, end-to-end distance, average over 19 individual hydrogen bond lengths, and Trp···His side chain distance, respectively.

3A,B. The results for the longer relaxation time constants (τ_2), assigned to the process of helix folding/unfolding, are 50–88 ns for AMBER03 at 320 K and 120–270 ns for OPLS/AA at 300 K. Within each simulation, time constants obtained with different methods are generally consistent within the statistical errors. The OPLS/AA relaxation times from RMSD, EEDIS, and HB fluctuations are only 10–30% below the experimental time of 300 ns at 298 K, essentially agreeing within the error estimates. The relaxation time based on WHDIS fluctuations is about 2.5 times lower than the measured value, a significant difference. On the basis of the trend in the experimental data, we can expect τ_2 values of about 100 ns at 320 K. The AMBER03 results are within a factor of 2 from this estimate.

Using two-state kinetics and the calculated helix fractions, we obtain folding times of $\tau_f = 90–110$ ns and unfolding times of $\tau_u =$

110–140 ns for AMBER03 at 320 K and $\tau_f = 720$ ns to $1.7\ \mu\text{s}$ and $\tau_u = 140–320$ ns for OPLS/A at 300 K. Similar results were obtained from a residence time analysis (see the Supporting Information). The OPLS/AA results are in good agreement with the values calculated from 298 K experimental data, $\tau_f = 680$ ns and $\tau_f = 540$ ns (see above).

The faster relaxation times τ_1 are in the 1–9 ns range in AMBER03 and the 11–16 ns range for OPLS/AA. The OPLS/AA results are very close to the experimental τ_1 value of 20 ns. On the basis of the trend in the experimental data, we would expect τ_1 values in the single nanoseconds at 320 K, and the AMBER03 results fall within this range.

It is especially interesting to analyze the relaxation of hydrogen bonds, which are crucial elements of α -helix structure. The dynamics of the individual hydrogen bonds along the peptide chain differ significantly— τ_1 values span 1–15 ns for AMBER03 and 2–82 ns for OPLS/AA, while the corresponding τ_2 values are 20–168 and 127–553 ns (see the Supporting Information). The slower relaxations vary by a factor of 8.4 in AMBER03 and 4.4 in OPLS/AA. The calculated τ_2 tend to vary relatively smoothly along the peptide chain, with a trend of faster relaxations at termini compared to the center, and with mostly similar relaxation times for neighboring residues. For OPLS/AA, a relatively large value of τ_2 was also found at the N-terminus, suggesting a stronger Trp···His interaction in this model (Supporting Information). This is somewhat different from values measured for a constrained photoswitchable peptide, in which more significant variations of relaxation times were found between neighboring residues.^{5c} The short times τ_1 from the average ACFs of hydrogen bond fluctuations (HB in Table 1) are 9 ns for AMBER03 and 12 ns for OPLS/AA, very similar to the measured experimental τ_1 results in this study. Although the hydrogen bond fluctuations shown in Figure 3A,B are averages over a wide range of time scales, they are well described by a two-exponential decay with the slow time constant τ_2 similar to those extracted from global coordinates—RMSD or EEDIS.

Another significant coordinate to consider is the tryptophan–histidine side chain distance (WHDIS in Table 1). This distance is directly probed in the T-jump experiments, which follow changes in Trp fluorescence due to quenching by His. Analysis of the data shows that the long relaxation time τ_2 obtained from WHDIS fluctuations is generally comparable to measures obtained from other coordinates but with the WHDIS times tending to be in the low range of calculated values (AMBER03) or the lowest of the calculated set (OPLS/AA). Thus, the tryptophan–histidine distance appears to provide a good representation of the global structure of the peptide, even though it involves only the N-terminal segment.

Previous explicit solvent simulations showed that qualitatively correct kinetics may be obtained for shorter systems, including WHS, for which the experimental $\tau_2 = 5$ ns.^{2f} Recently, a folding relaxation time of about 15 ns was obtained for a 12-residue helix with AMBER03 at 300 K.⁸ Our results indicate that realistic kinetics may also be modeled for the longer WH21 peptide.

Transitions: Average Path. A statistical picture of helix folding is shown in Figure 2C,D. This shows the populations of the individual hydrogen bonds of WH21, HB1–HB19, evaluated along the reaction coordinate describing the total number of helical hydrogen bonds present, $\text{NHB} = 0, \dots, 19$. This picture is essentially identical to the one obtained previously from our REMD simulations of WH21.^{3a} Both AMBER03 and OPLS/AA MD results show the unfolding of the helix is initiated at the termini, leading to an “off-center” intermediate with high

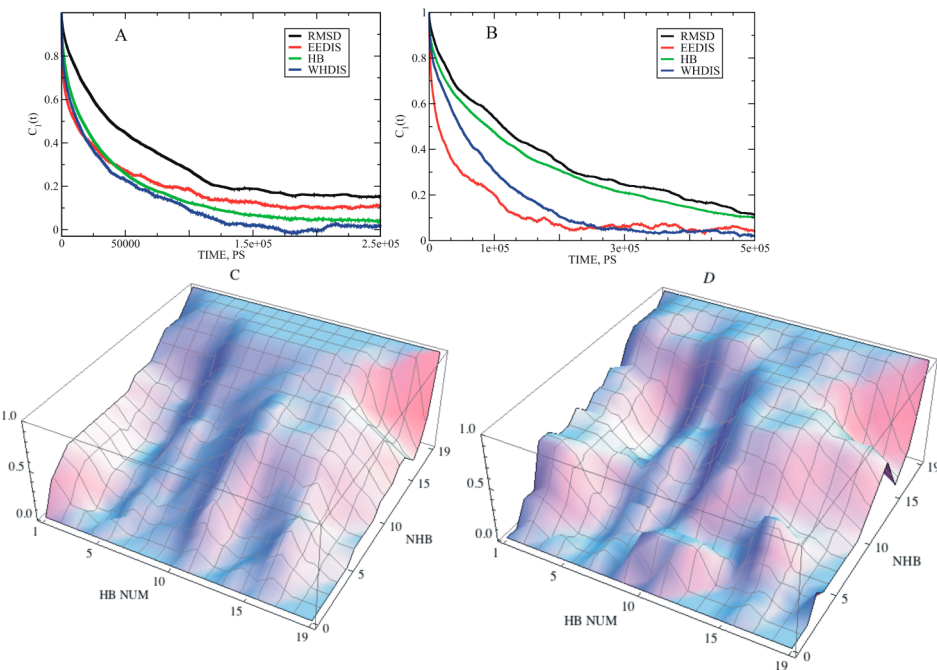


Figure 3. Autocorrelation functions of fluctuations in (A) 16.9 μ s AMBER03 MD at 320 K and (B) 13 μ s OPLS/AA MD at 300 K. Statistical folding pathways (C) AMBER03 and (D) OPLS/AA.

populations of hydrogen bonds HB11–HB16. In the final stages of unfolding (or initial stages of folding), there appears to be some preferential helix initiation at HB1, HB6, HB11, and HB16. The MD results tend to exhibit more noise than the REMD ones, suggesting that more complete sampling may have been obtained in REMD.^{3a}

Transitions: Individual Paths. A detailed description of the individual helix–coil transition paths found in our MD simulations is provided in the Supporting Information. Overall, we have sampled 70 transitions, 35 folding and 35 unfolding, with each following a unique path. The individual transitions were quite complex, with individual hydrogen bonds undergoing several breaking/formation events within each pass. A simplified description of the paths is given in Table 2 and examples of

unfolded region expanding to the C-terminus and finally to the N-terminus. The intermediate structures, corresponding to $NHB = 9–10$, involve primarily one (43%) or two helical segments (47%), with a small fraction of three-helix conformers (Table 2). In the OPLS/AA simulation, the N-terminal path 1 is most favored, followed by 71% of all transitions, with smaller contributions from paths 2 and 3, while the central path 4 is not detected. In this case, the intermediates with $NHB = 9, 10$ were either single helices (53%) or two-helix forms (47%). Three-helix conformers were not found in OPLS/AA MD. Examples of the four paths are shown in Figure 4.

Overall, the individual transitions provide a more complex picture than that presented by the average path, showing that several separate components contribute to the mean. In the AMBER03 case, the presence of path 4, followed by 28% of all transitions and involving unfolding initiation in the peptide center, is not evident in the average path (see Figure 3). However, most of the paths (72% in AMBER03 and 100% in OPLS/AA) are initiated at the termini. Therefore, the presence of intermediate structures with highly populated hydrogen bonds HB11–16 is consistent with the detected transitions. The two force fields used in these simulations generally agree on the unfolding path details. The three paths found in OPLS/AA are also seen in AMBER03, and single-helix and two-helix intermediates dominate in both cases. However, the AMBER03 results differ from OPLS/AA by predicting the additional central folding pathway and a small but detectable contribution from three-helix intermediates.

Previous helix folding path analyses were primarily based on implicit solvent simulations, suggesting the presence of two-stage or three-stage folding.^{5a,b} The presence of intermediates with three short helix fragments was observed by Pande et al. for model 21-residue alanine-rich peptides with a modified AMBER99 potential in explicit water.⁶ Recently, a kinetic network analysis based on implicit solvent MD was presented for folding of a constrained helix.^{5c} In addition, the analysis of WH21

Table 2. Summary of Sampled Helix–Coil Transition Paths^a

	path 1, N-term	path 2, C-term	path 3, zipper	path 4, central	intermediates 1H/2H/3H
AMBER03	23%	28%	21%	28%	43% /47%/10%
OPLS/AA	71%	23%	6%		53%/47%/-

^aNumbers of sampled transitions were 53 (26 folding and 27 unfolding) in AMBER03 simulations and 17 (9 folding and 8 unfolding) in OPLS/AA. Labeling of intermediates: 1H, single helices; 2H, two-helix structures; 3H, three-helix structures.

transitions shown in Figure 4. These paths are all analyzed in the unfolding direction for clarity. In the AMBER03 MD simulations, four main paths were sampled, with roughly equal frequencies. In path 1 (N-terminal), the first unfolded section appears at the N-terminal, and then a second unfolded region builds up at the C-terminus and the two unfolded segments expand to encompass the complete peptide. In path 2 (C-terminal), the C-terminus unfolds first, followed by the N-terminus and central region. Path 3 (zipper) involves mostly consecutive unfolding from the C-terminus to N-terminus. In path 4 (central), unfolding starts in the central section, with the

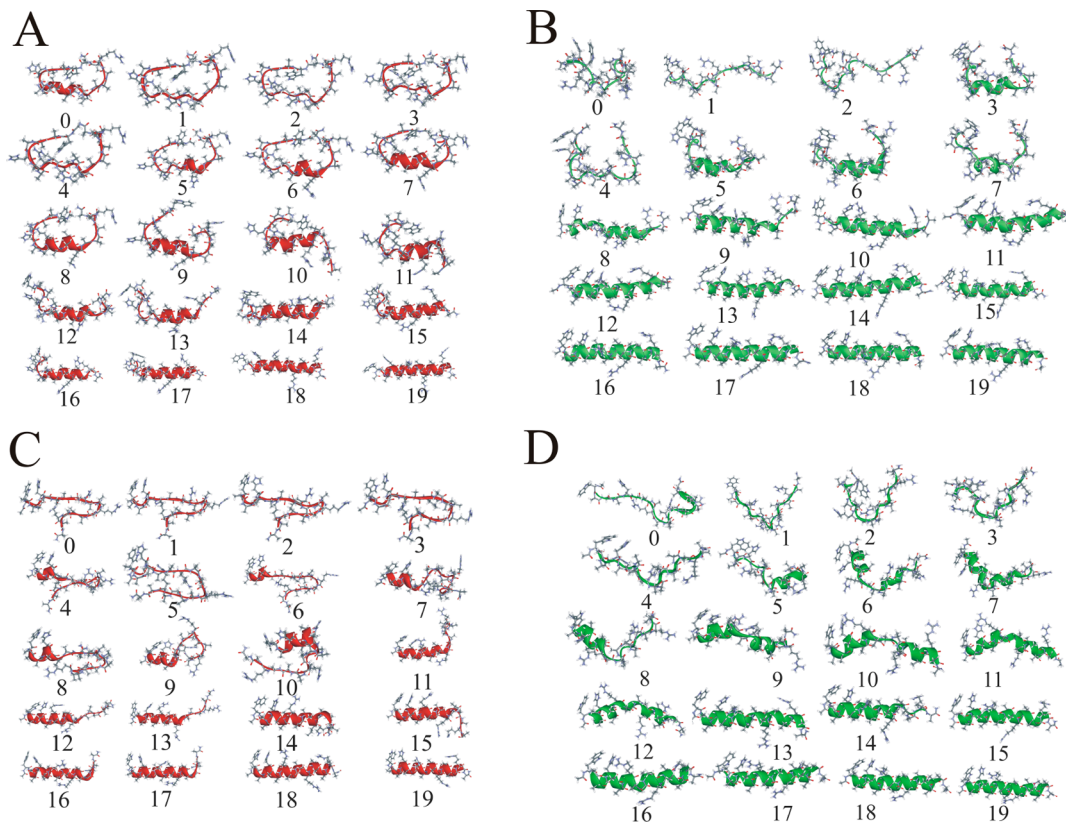


Figure 4. Examples of four types of folding paths from WH21 trajectories: (A) N-terminal path 1; (B) C-terminal path 2; (C) zipper path 3; (D) central path 4. Transitions analogous to paths 1–3 were found in both AMBER03 and OPLS/AA trajectories.

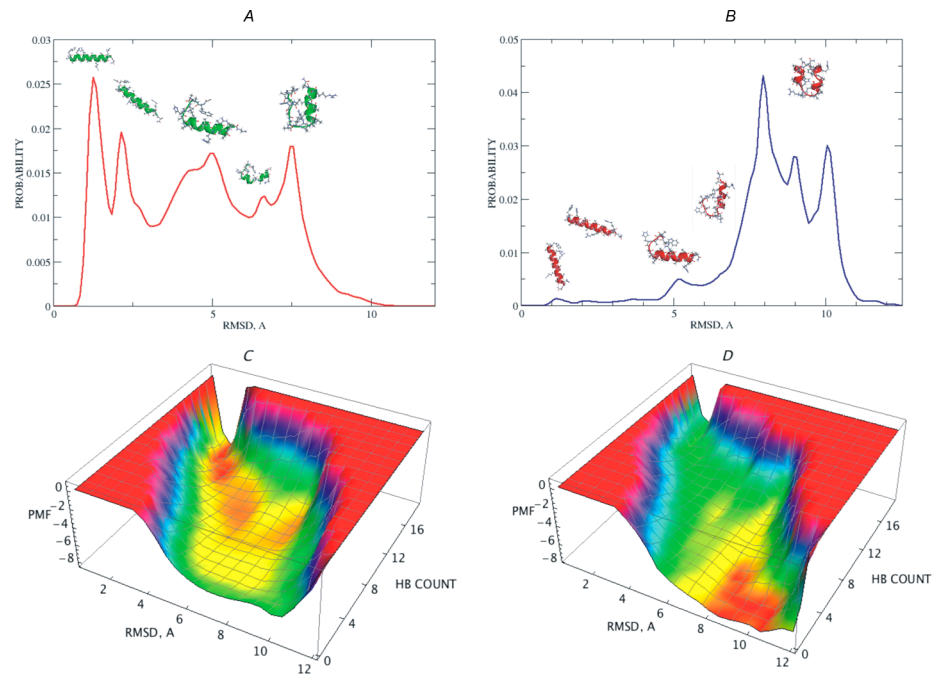


Figure 5. Most highly populated intermediates as a function of $C\alpha$ RMSD from an ideal helix: (A) AMBER03; (B) OPLS/AA. Free energy landscapes in coordinates of RMSD from helix and hydrogen bond count: (C) AMBER03; (D) OPLS/AA. PMF in kcal/mol.

folding along several paths using milestoning showed that the N-terminal path was in best agreement with experimental data, in accord with our OPLS/AA results.⁹

Intermediate Structures. To analyze the helix folding pathway in more detail, we have performed clustering of the

sampled structures of WH21 for different values of $C\alpha$ RMSD from helix. The results are shown in more detail in the Supporting Information, while the most highly populated clusters are schematically presented in Figure 5A,B and described below. In the AMBER03 trajectory, initial unfolding, with RMSD

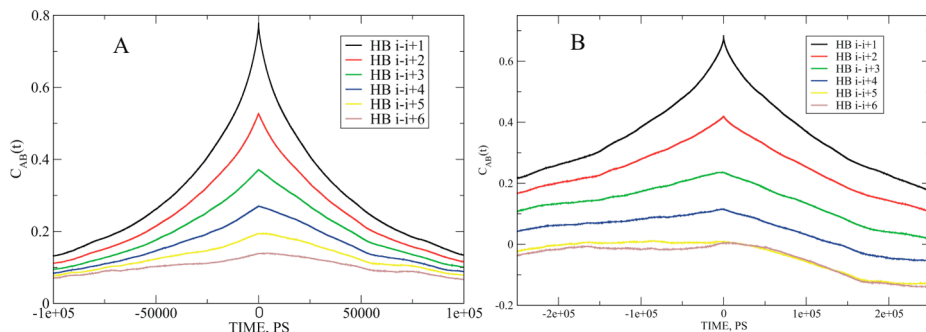


Figure 6. Correlations between fluctuations of hydrogen bonds: $i - i + 1$, nearest neighbors; $i - i + 2$, next-nearest neighbors; etc.: (A) AMBER03; (B) OPLS/AA.

$\approx 2\text{--}3 \text{ \AA}$ and NHB $\approx 15\text{--}16$, occurs primarily at both termini (Figure 5A). This is followed by unfolding of the N-terminal region, with significant population of an intermediate structure with a single C-terminal helix, with RMSD $\approx 5 \text{ \AA}$ and NHB ≈ 11 , which roughly agrees with the statistical analysis from Figure 3. Next is formation of a helix-turn-helix structure with short helices located in the central and C-terminal regions at RMSD $\approx 6 \text{ \AA}$ and NHB $\approx 8\text{--}9$ and a coil–helix hairpin with a C-terminal helix at RMSD $\approx 8 \text{ \AA}$ and NHB $\approx 4\text{--}5$. Finally, at RMSD $\approx 10 \text{ \AA}$, solely fully unfolded structures are sampled.

The major sampled intermediates at the start of unfolding are very similar in OPLS/AA and AMBER03 trajectories. In OPLS/AA, initial stages of unfolding also involve unwinding at the two termini, followed by a formation of a single C-terminal helix with RMSD $\approx 5 \text{ \AA}$ and NHB ≈ 10 (Figure 5B). Next is the appearance of a coil–helix structure with a short C-terminal helix at RMSD $\approx 6 \text{ \AA}$ and NHB $\approx 6\text{--}7$ and a helix-turn-helix hairpin at RMSD $\approx 8 \text{ \AA}$ and NHB ≈ 4 , and fully unfolded structures are sampled at RMSD $\approx 10 \text{ \AA}$. The order of appearance of the helix–coil hairpin and helix-turn-helix motifs are thus reversed in the two force fields.

Free Energy Landscapes. The free energy landscapes in coordinates of $C\alpha$ RMSD from helix and number of helical hydrogen bonds are shown in Figure 5C,D. For AMBER03, there is a clear free energy minimum in the folded region, lying in a narrow valley of states with RMSD $\approx 1\text{--}3 \text{ \AA}$ and NHB $\approx 15\text{--}19$. Additionally, there is a broad range of populated intermediates of comparable stability, with RMSD $\approx 3\text{--}6 \text{ \AA}$ and NHB $\approx 8\text{--}14$, and another broad region of mostly unfolded states with RMSD $> 6 \text{ \AA}$ and NHB < 8 . The barriers separating the folded, intermediate, and unfolded basins are quite low, below 0.5 kcal/mol. For OPLS/AA, the main free energy minimum corresponds to unfolded states with RMSD $> 6 \text{ \AA}$ and NHB < 8 . There is also a broad basin of intermediates and a narrow region of folded states. The landscape is tilted up from the most stable coil forms to the least stable helices, with barriers of about 1.5 kcal/mol between intermediates and folded states, and about 1 kcal/mol between intermediates and unfolded states. These landscapes are similar to the ones obtained from REMD of WH21.^{3a}

Hydrogen Bond Correlations. Cross-correlation functions $\langle \Delta R_i(0)\Delta R_j(t) \rangle$ of hydrogen bond length fluctuations from the entire trajectories are shown in Figure 6. These results show highest correlations occurring at equal time ($t = 0$) and decaying for both preceding and following times, with time constants of ca. 50 ns for the 320 K AMBER03 and ca. 100 ns for the 300 K OPLS/AA simulation. These time scales are comparable to the corresponding slow relaxation times. The $t = 0$ correlations are very high for nearest neighbors, 0.8 in AMBER03 and 0.7 in

OPLS/AA. Significant correlations exhibit a range of ca. 4 nearest neighbors in AMBER03 and ca. 3 nearest neighbors in OPLS/AA. The correlations are also generally symmetric for times $t < 0$ and > 0 , with some slight asymmetry appearing only for the lowest values of $C(t) < 0.1$. Similar values of the static correlation coefficient are obtained over transition regions only (Supporting Information).

In a time-resolved IR study of a constrained helix, it was argued that the large variation in correlation times of consecutive hydrogen bonds indicates independent, noncooperative folding.^{3c} For our unconstrained peptide, we find a smaller overall range and smoother variation with position for the longer correlation times, which indicate the presence of a partial cooperativity of folding. Taken together with the detected correlations of hydrogen bond fluctuations, we suggest that the experimentally observed short relaxation time might correspond to joint folding/unfolding transitions of several neighboring hydrogen bonds, rather than individual hydrogen bond dynamics.

CONCLUSIONS

By a combination of improved experimental measurements and a detailed microscopic description provided by modeling, we have obtained new insights into the helix folding process of the WH21 peptide. Temperature jump kinetic studies with improved time resolution were performed at several temperatures, revealing the presence of relaxation with two time constants which fall in the 10 and 100 ns range near room temperature. This clearly shows that the process cannot be fully described by a two-state model, and an additional fast process contributes to helix folding. In the computational studies, we performed multi-microsecond molecular dynamics simulations of WH21 in explicit water with AMBER03 and OPLS/AA potentials. The simulations yielded values of helix content and two kinetic time constants in quite good agreement with the experimental data, showing that current simulation methods provide realistic models of peptide structure and dynamics, lending credence to the uncovered microscopic details.

Our most important microscopic finding is the description of the different paths contributing to the helix–coil transition. For both force fields, three main transition paths were found, initiated at the termini. An additional fourth path starting in the central region and expanding to the termini was detected only with AMBER03. The great majority of the structures sampled in the MD were a widely diverse set of folding intermediates. Detailed analysis showed the presence of several characteristic intermediate conformers for WH21 unfolding—a central helix with frayed ends at the beginning, an “off-center” helix in the C-

terminal region in the middle stage, and short helix–coil hairpin and helix-turn-helix motifs toward the end of the process. The presence of intermediates has appeared in recent simulations of loop closure dynamics²² and β -hairpin folding.²³

The short relaxation time τ_1 from the T-jump experiments was quite similar to the average fast relaxation of individual hydrogen bonds in our trajectories. Also, detailed analysis of the hydrogen bond fluctuations showed the presence of partial cooperativity, with neighboring bonds exhibiting correlated transitions and similar relaxation times. This leads us to propose that the fast time τ_1 be assigned to cooperative transitions of groups of neighboring hydrogen bonds. Overall, the MD simulations show that the WH21 peptide samples a very large number of conformations, of which most are folding intermediates. The motion may be described as conformational diffusion on a flat free energy landscape with correlated transitions of neighboring hydrogen bonds occurring on a 10 ns time scale and overall folding on a 100 ns time scale.

The two force fields used—AMBER03 and OPLS/AA—generally yielded comparable results for helix content, peptide dynamics, and transition paths. Some differences in predictions did emerge. These included the presence of the fourth (central) unfolding path and population of 3-helix intermediates in AMBER03 only, details of the structure of the intermediates, and the markedly slower relaxation of the N-terminal hydrogen bond HB1 in OPLS/AA. The complex process of helix folding still requires more experimental and modeling studies to unravel all of its secrets.

■ ASSOCIATED CONTENT

§ Supporting Information

Additional figures and tables describing details of the simulation data. This material is available free of charge via the Internet at <http://pubs.acs.org>.

■ AUTHOR INFORMATION

Corresponding Authors

*E-mail: 112gjas@uccaribe.edu (G.S.J.).

*E-mail: kkuczera@ku.edu (K.K.).

Notes

The authors declare no competing financial interest.

■ ACKNOWLEDGMENTS

G.S.J. would like to thank William A. Eaton for allowing access to the nanosecond laser temperature jump apparatus. We acknowledge Baylor University for access to computer resources. G.S.J. would also like to thank Wilson Veras and Elizabeth De Leon. This project was supported in part by a subaward for DOE grant DE-FG02-08ER46528 for K.K.

■ REFERENCES

- (a) Onuchic, J. N.; Luthey-Schulten, Z.; Wolynes, P. G. Theory of protein folding: The energy landscape perspective. *Annu. Rev. Phys. Chem.* **1997**, *48*, 545–600. (b) Dobson, C. M.; Sali, A.; Karplus, M. Protein folding: A perspective from theory and experiment. *Angew. Chem., Int. Ed.* **1998**, *37* (7), 868–893. (c) Thirumalai, D.; Klimov, D. K. Deciphering the timescales and mechanisms of protein folding using minimal off-lattice models. *Curr. Opin. Struct. Biol.* **1999**, *9* (2), 197–207.
- (a) Williams, S.; Causgrove, T. P.; Gilmanshin, R.; Fang, K. S.; Callender, R. H.; Woodruff, W. H.; Dyer, R. B. Fast events in protein folding: Helix melting and formation in a small peptide. *Biochemistry* **1996**, *35* (3), 691–697. (b) Thompson, P. A.; Eaton, W. A.; Hofrichter, J. Laser temperature jump study of the helix reversible arrow coil kinetics of an alanine peptide interpreted with a ‘kinetic zipper’ model. *Biochemistry* **1997**, *36* (30), 9200–9210. (c) Thompson, P. A.; Munoz, V.; Jas, G. S.; Henry, E. R.; Eaton, W. A.; Hofrichter, J. The helix-coil kinetics of a heteropeptide. *J. Phys. Chem. B* **2000**, *104* (2), 378–389. (d) Lednev, I. K.; Karnoup, A. S.; Sparrow, M. C.; Asher, S. A. alpha-helix peptide folding and unfolding activation barriers: A nanosecond UV resonance raman study. *J. Am. Chem. Soc.* **1999**, *121* (35), 8074–8086. (e) Mohammed, O. F.; Jas, G. S.; Lin, M. M.; Zewail, A. H. Primary Peptide Folding Dynamics Observed with Ultrafast Temperature Jump. *Angew. Chem., Int. Ed.* **2009**, *48* (31), 5628–5632. (f) Lin, M. M.; Mohammed, O. F.; Jas, G. S.; Zewail, A. H. Speed limit of protein folding evidenced in secondary structure dynamics. *Proc. Natl. Acad. Sci. U.S.A.* **2011**, *108* (40), 16622–16627. (g) Jas, G. S.; Hegefled, W. A.; Majek, P.; Kuczera, K.; Elber, R. Experiments and comprehensive simulations of the formation of a helical turn. *J. Phys. Chem. B* **2012**, *116* (23), 6598–6610.
- (a) Jas, G. S.; Kuczera, K. Computer simulations of helix folding in homo- and heteropeptides. *Mol. Simul.* **2012**, *38* (8–9), 682–694.
- (b) Gnanakaran, S.; Nymeyer, H.; Portman, J.; Sanbonmatsu, K. Y.; Garcia, A. E. Peptide folding simulations. *Curr. Opin. Struct. Biol.* **2003**, *13* (2), 168–74. (c) Brooks, C. L., 3rd. Protein and peptide folding explored with molecular simulations. *Acc. Chem. Res.* **2002**, *35* (6), 447–454.
- (d) Garcia, A. E.; Sanbonmatsu, K. Y. Alpha-helical stabilization by side chain shielding of backbone hydrogen bonds. *Proc. Natl. Acad. Sci. U.S.A.* **2002**, *99* (5), 2782–2787.
- (e) (a) Zhang, W.; Lei, H. X.; Chowdhury, S.; Duan, Y. Fs-21 peptides can form both single helix and helix-turn-helix. *J. Phys. Chem. B* **2004**, *108* (22), 7479–7489. (b) Ferrara, P.; Apostolakis, J.; Caflisch, A. Thermodynamics and kinetics of folding of two model peptides investigated by molecular dynamics simulations. *J. Phys. Chem. B* **2000**, *104* (20), 5000–5010. (c) Ihala, J. A.; Paoli, B.; Muff, S.; Backus, E. H. G.; Bredenbeck, J.; Woolley, G. A.; Caflisch, A.; Hamm, P. alpha-Helix folding in the presence of structural constraints. *Proc. Natl. Acad. Sci. U.S.A.* **2008**, *105* (28), 9588–9593.
- (f) Sorin, E. J.; Pande, V. S. Exploring the helix-coil transition via all-atom equilibrium ensemble simulations. *Biophys. J.* **2005**, *88* (4), 2472–2493.
- (g) (a) Buchete, N. V.; Hummer, G. Coarse master equations for peptide folding dynamics. *J. Phys. Chem. B* **2008**, *112* (19), 6057–6069. (b) Hegefled, W. A.; Chen, S. E.; DeLeon, K. Y.; Kuczera, K.; Jas, G. S. Helix Formation in a Pentapeptide Experiment and Force-field Dependent Dynamics. *J. Phys. Chem. A* **2010**, *114* (47), 12391–12402.
- (h) von Hansen, Y.; Kalcher, I.; Dzubiella, J. Ion Specificity in alpha-Helical Folding Kinetics. *J. Phys. Chem. B* **2010**, *114* (43), 13815–13822.
- (i) Kuczera, K.; Jas, G. S.; Elber, R. Kinetics of Helix Unfolding: Molecular Dynamics Simulations with Milestoning. *J. Phys. Chem. A* **2009**, *113* (26), 7461–7473.
- (j) (a) Marqusee, S.; Robbins, V. H.; Baldwin, R. L. Unusually Stable Helix Formation in Short Alanine-Based Peptides. *Proc. Natl. Acad. Sci. U.S.A.* **1989**, *86* (14), 5286–5290. (b) Munoz, V.; Serrano, L. Helix Design, Prediction and Stability. *Curr. Opin. Biotechnol.* **1995**, *6* (4), 382–386.
- (k) Graf, J.; Nguyen, P. H.; Stock, G.; Schwalbe, H. Structure and dynamics of the homologous series of alanine peptides: A joint molecular dynamics/NMR study. *J. Am. Chem. Soc.* **2007**, *129* (5), 1179–1189.
- (l) Ianoul, A.; Mikhonin, A.; Lednev, I. K.; Asher, S. A. UV resonance Raman study of the spatial dependence of alpha-helix unfolding. *J. Phys. Chem. A* **2002**, *106* (14), 3621–3624.
- (m) Huang, C. Y.; Getahun, Z.; Zhu, Y. J.; Klemke, J. W.; DeGrado, W. F.; Gai, F. Helix formation via conformation diffusion search. *Proc. Natl. Acad. Sci. U.S.A.* **2002**, *99* (5), 2788–2793.
- (n) Jas, G. S.; Eaton, W. A.; Hofrichter, J. Effect of viscosity on the kinetics of alpha-helix and beta-hairpin formation. *J. Phys. Chem. B* **2001**, *105* (1), 261–272.

(15) Schuler, B.; Lipman, E. A.; Steinbach, P. J.; Kumke, M.; Eaton, W. A. Polyproline and the “spectroscopic ruler” revisited with single-molecule fluorescence. *Proc. Natl. Acad. Sci. U.S.A.* **2005**, *102* (8), 2754–2759.

(16) Brooks, B. R.; Brooks, C. L.; Mackerell, A. D.; Nilsson, L.; Petrella, R. J.; Roux, B.; Won, Y.; Archontis, G.; Bartels, C.; Boresch, S.; Caflisch, A.; Caves, L.; Cui, Q.; Dinner, A. R.; Feig, M.; Fischer, S.; Gao, J.; Hodoscek, M.; Im, W.; Kuczera, K.; Lazaridis, T.; Ma, J.; Ovchinnikov, V.; Paci, E.; Pastor, R. W.; Post, C. B.; Pu, J. Z.; Schaefer, M.; Tidor, B.; Venable, R. M.; Woodcock, H. L.; Wu, X.; Yang, W.; York, D. M.; Karplus, M. CHARMM: The Biomolecular Simulation Program. *J. Comput. Chem.* **2009**, *30* (10), 1545–1614.

(17) Duan, Y.; Wu, C.; Chowdhury, S.; Lee, M. C.; Xiong, G.; Zhang, W.; Yang, R.; Cieplak, P.; Luo, R.; Lee, T.; Caldwell, J.; Wang, J.; Kollman, P. A point-charge force field for molecular mechanics simulations of proteins based on condensed-phase quantum mechanical calculations. *J. Comput. Chem.* **2003**, *24* (16), 1999–2012.

(18) Kaminski, G. A.; Friesner, R. A.; Tirado-Rives, J.; Jorgensen, W. L. Evaluation and reparametrization of the OPLS-AA force field for proteins via comparison with accurate quantum chemical calculations on peptides. *J. Phys. Chem. B* **2001**, *105* (28), 6474–6487.

(19) Hess, B.; Kutzner, C.; van der Spoel, D.; Lindahl, E. GROMACS 4: Algorithms for highly efficient, load-balanced, and scalable molecular simulation. *J. Chem. Theory Comput.* **2008**, *4* (3), 435–447.

(20) Sagui, C.; Darden, T. A. Molecular dynamics simulations of biomolecules: Long-range electrostatic effects. *Annu. Rev. Biophys. Biomol. Struct.* **1999**, *28*, 155–179.

(21) Di Pierro, M.; Elber, R. Automated Optimization of Potential Parameters. *J. Chem. Theory Comput.* **2013**, *9* (8), 3311–3320.

(22) Daidone, I.; Neuweiler, H.; Doose, S.; Sauer, M.; Smith, J. C. Hydrogen-Bond Driven Loop-Closure Kinetics in Unfolded Polypeptide Chains. *PLoS Comput. Biol.* **2010**, *6*, 1.

(23) Thukral, L.; Daidone, I.; Smith, J. C. Structured Pathway across the Transition State for Peptide Folding Revealed by Molecular Dynamics Simulations. *PLoS Comput. Biol.* **2011**, *7*, 9.